Stability and Dynamical Analysis of the Davey–Stewartson Model

Muhammad Moneeb Tariq[1*], Muhammad Aziz ur Rehman[1], and Muhammad Bilal Riaz[2]

[1]Department of Mathematics, University of Management and Technology, Lahore, Pakistan
[2]IT4Innovations, VSB – Technical University of Ostrava, Ostrava, Czech Republic;, ,
Corresponding author*: chmoneeb136@gmail.com

Abstract

This study investigates the nonlinear coupled Davey-Stewartson Fokas system, a mathematical model describing pulse propagation in monomode optical fibers. Employing a powerful analytical technique, we derive novel periodic and solitary wave solutions, including bright, dark, periodic, kink soliton, and exponential soliton solutions. These solutions significantly advance our understanding of the precise dynamics of solitons in nonlinear optics. The proposed methods effectively discover and characterize new solitary wave solutions, providing deeper insights into the model's behavior. These computational techniques hold enormous promise for various scientific applications and enhance our knowledge of fundamental dynamics. This paper visually represents soliton solutions in the form of 2D, 3D, and contour plots. By applying the Galilean transformation and using appropriate parameter values, we obtain the planar dynamical system, which aids in the dynamical analysis of the Davey-Stewartson Fokas system. Using the planer dynamical system to examine the phase-portrait analysis of the system. Also examine the sensitivity analysis of the system's reaction to various initial conditions during both the initial and intransitive phases. Furthermore, we investigate the chaotic behavior by adding an external force, examining whether the planar dynamical system exhibits periodic, quasi-periodic, or chaotic patterns.

Keywords: Davey stewartson system, The modified Khater method, Bifurcation analysis, Sensitivity analysis, Chaotic behavior

1 Introduction

In the real world, a wide range of systems exhibit nonlinearity and undergo changes over time. When time consistently varies, we obtain mathematical expressions in the form of nonlinear partial differential equations (NLPDE). These equations have various applications in the fields of physics, biology, mathematics and engineering. They are essential for comprehending nonlinear phenomena, simulating biological processes, and studying the dynamics of engineering systems [1, 2]. PDEs play a critical role in engineering by facilitating the design of structures and process optimization. They are particularly important in fields such as aerodynamics for aircraft design and structural analysis in civil engineering. Moreover, in the field of finance, PDEs play a crucial role by determining option prices and effectively managing risk through the Black-Scholes equation[3].

There are numerous approaches to analyze nonlinear evolutionary equations (NLEEs) in order to obtain accurate solutions. Researchers have developed a variety of reliable and effective mathematical techniques, including the modified Khater method [5], the modified F-expansion method [6], the improved Bernoulli sub-equation function method [7], the Hirota bilinear method [8], the local meshless method [9], the Lie group method [10], the tanh–sech method [11], and several others [12]-[17]. Hossain et al. applied the enhanced (G'/G)-expansion method to investigate the traveling wave solutions of NLEEs [18]. Saifullah et al. [19] used Hirota bilinear technique to show the soliton interaction for the perturbed KdV equation. Novikov et al. investigated the soliton theory by employing the inverse scattering technique [20]. Roshid utilised the Mean Squared Error (MSE) approach to examine the novel precise solutions of a set of nonlinear equations governing shallow water [21]. Kumar et al. [22] used the symmetry analysis approach to study the multi-solution solutions of a Boussinesq problem. The Kyoto school [23] initially developed the Kadomtsev-Petviashvili (KP) hierarchy reduction approach, which Ohta et al. [24] later enhanced. The KP equation is a nonlinear equation that governs the behaviour of shallow water waves in two dimensions. Several solvable dynamic equations, including the nonlinear Schrödinger (NLS) problem have employed this methodology [25, 26]. Soliton solutions, which are found in nonlinear phemonena, exhibit a diverse range of properties and soliton solutions. Over the past few decades, numerous scholars have examined soliton solutions and various forms of integrable equations. Certain nonintegrable equations also possess solutions. Moreover, other investigations have demonstrated the existence of certain solutions and alternative forms of precise solutions to nonlinear integrable equations. However, scholars use several strategies to construct interaction phenomena for nonlinear evolution models, especially for equations with constant coefficients. However, there is still a large gap in this direction. Thus, studying several equations with varied characteristics and forms is essential to developing many additional physical traits and properties. [27, 28].

Optical soliton pulses are crucial in soliton communication technology, enabling effective transmission of data over long distances across oceans and continents in the telecommunications sector [29]. Because the Davey-Stewartson equations (DSE) are important for studying turbulence in plasma waves or optical fibres, the exact optical soliton solutions help us understand a number of interesting physical phenomena. This work focuses on analysing the impact of noise on the coupled DSE. Davey and Stewartson formulated the DSE in 1974. We employ the DSE technique to demonstrate the temporal evolution of a three-dimensional wave packet in shallow water. In optics, the DS Fokas system serves as a significant physical model that explains the nonlinear propagation of pulses in monomode optical fibres. Kumar and Kumar [30] resolved the DS Fokas system using the generalised Riccati equation mapping technique and the generalised Kudryashov method. Khater [31] used the ansatz approach and projective Riccati expansion method to investigate the DS Fokas system, resulting in many solitary wave solutions. Chen et al. [32] derived the soliton solutions by employing the Hirota bilinear approach. Ohta et al. examined the dynamics of rogue waves in the DSE [33]. Fokas et al. study the dromions and a boundary value problem for the DSE [34]. Selima examines surface wave propagation in shallow water: a nonlinear dispersive DS system and its stability [35]. Rehman et al. investigated the solitary wave behavior of (4+1)-dimensional DS equation using various techniques [36]. Mihalache et al. [37] studied the nonlocal DSE with completely space shifted PT-symmetry and to find the wave behavior that enhance our understanding.

Our main goal in this study, to generate novel solitary wave solutions using the modified Khater method (MKM). The MKM is a renowned approach for obtaining precise solutions to nonlinear dynamical systems. This approach offers many types of soliton solutions that enhance our understanding of the wave phenomena in physical systems, including dark soliton that show the dips on a continuous wave, bright soliton that shows the increase in the intensity of wave, combined dark-bright soliton, and periodic wave that show the reputation of wave pattern in system. This methodology is more effective than others and provides us with superior solutions. Furthermore, these findings are highly impactful when examining the DS model at the microlevel, revealing the behavior of the dynamical system in response to noise. These results represent traditional solutions in the optical fiber communication system. Additionally, we explain the characteristics of the newly obtained solutions by creating visual representations in the form of 3D and 2D graphs. These graphs aid in comprehending the related physical events.

The article is structured as follows: Section 2 introduces the equation's formulation, highlighting its conceptual framework. Section 3 provides a comprehensive explanation of the modified Khater method. In Section 4, traveling wave solutions are discussed, accompanied by graphical illustrations. In Section 5 explain the stability analysis and Section 6 explores the dynamical analysis, featuring graphical depictions of the system's behavior for different initial conditions. Finally, Section 6 concludes the study by summarizing the findings of the proposed model.

2 Modified Khater Method

The MKM is a technique used for solving differential equations, particularly those arising in physical and engineering problems. The method entails setting initial conditions and parameters, then applying a specific formula to find the solution. Scholar use this method for its efficiency and accuracy in handling NLPDE. MKM apply [5] as a technique to create a novel wave pattern for a hypothetical model. Some specific details about this method are as follows:

$$F(u, u_x, u_t, u_{xx}, u_{xt}, u_{tt}, ...\omega_x, \omega_y, \omega_t.....) = 0. \tag{1}$$

Where $\omega = \omega(x, y, t)$ and $u = u(x, y, t)$ is unknown function.

Step 1: Select the transformation

$$u(x, y, t) = e^{is}U(\xi), \omega(x, y, t) = W(\xi), \xi = mx + ay - nt, s = fx + gy + ht. \tag{2}$$

Which convert the PDEs into ODEs.

$$G(U, U', U'', U''', ...U^n) = 0. \tag{3}$$

Step 2 : Suppose the general solution to the ODE is

$$U(\xi) = \sum_{j=0}^{N} \Lambda_j \mathfrak{U}^j(\xi). \tag{4}$$

where $\mathfrak{U}^j(\xi)$ is the solution of the equation and Λ_j $(0 \leq \mathrm{j} \leq \mathrm{n})$ are the constants:

$$\mathfrak{U}'(\xi) = ln(v)(b_1 + b_2\mathfrak{U}(\xi) + b_3\mathfrak{U}^2(\xi)). \tag{5}$$

Where $v \neq 0, 1$ and b_1, b_2 and b_3 are constant.

Step 3 : By using the balancing technique to determine the balance number N, comparing the highest derivative and the nonlinear term.

Step 4 : Using Eq. (5) with Eq. (4) in Eq. (3) to obtain an algebraic equation with different power of $\mathfrak{U}(\xi)$. Equating the power $\mathfrak{U}(\xi)$ to zero and determining the values of Λ by solving the algebraic equation.

3 Governing Equation

The nonlinear coupled DS Fokas system is a significant mathematical model used to describe pulse propagation in monomode optical fibers, and recent research has made notable advancements in understanding its dynamics and solutions. Researchers have introduced new mathematical techniques to investigate this system, concentrating on generating various optical wave solutions like dark solitons and periodic waveforms, which improve our understanding of wave propagation behavior. We investigated the nonlinear Fokas equation, an integrable extension of the KP and DS equations, for its applications in modeling surface. This study focuses on investigating the (2+1)-dimensional nonlinear coupled DS Fokas system. The DS Fokas system is a key physical model in optics that helps to explain pulse movement in monomode optical fibres [38].

$$i\frac{\partial u}{\partial t} + \alpha_1 \frac{\partial^2 u}{\partial x^2} + \alpha_2 u\omega = 0, \tag{6}$$

$$\alpha_3 \frac{\partial w}{\partial y} - \alpha_4 \frac{\partial |u|^2}{\partial x} = 0. \tag{7}$$

The complex value functions u and w represent nonlinear pulse propagation in monomode optical fibers. The non-zero free constants are α_1, α_2, α_3, and α_4 which affect the behavior of dynamic optical waves. The α_1 is a parameter that shows the dispersion of the model. It is used to measure the dispersion of the system. The α_2 is the nonlinearity coupling parameter, the parameter is used to measure the intensity of the nonlinear interaction between the two components of the system. The parameter, α_3, represents the transverse dispersion parameter that represents the degree of dispersion along the transverse direction. Lastly, parameter α_4 is nonlinearity saturation and the amount of saturation in the nonlinear interaction. The transformation wave is well selected to enable the analysis and resolution of the system. The method used to reduce the original problem systematically, which allows the equations to be rewritten in a more solvable form.

We achieved the following equation by applying the wave transformation Eq. (2) into Eq. (6) and Eq. (7).

Real part

$$m^2\alpha_1 U''(\xi) - (f^2\alpha_1 + h)U(\xi) + \alpha_2 U(\xi)W(\xi) = 0, \tag{8}$$

imaginary part

$$(2fm\alpha_1 - n)U'(\xi) = 0. \tag{9}$$

Using Eq. (9) we have,

$$n = 2fm\alpha_1. \tag{10}$$

Again substitute Eq. (8) into Eq.(7) and we have,

$$a\ \alpha_3 W'(\xi) - 2m\alpha_4 U(\xi)U'(\xi) = 0. \tag{11}$$

By simplifying Eq. (11) we get,

$$W(\xi) = \frac{m\alpha_4}{\alpha_3 a}U^2(\xi). \tag{12}$$

Using Eq. (12) in Eq. (8), written in the form

$$U''(\xi) + \lambda U(\xi) + \beta U^3(\xi) = 0. \tag{13}$$

Where $\lambda = \left(-\frac{f^2\alpha_1 + h}{m^2\alpha_1}\right)$ and $\beta = \left(\frac{\alpha_2\alpha_4}{ma\alpha_1\alpha_3}\right)$. f, α_1, α_2, α_3, α_4, m, and h are real constant.

4 Traveling Wave Solution

In this section, we derive the soliton solutions of Eq. (13) by utilizing the wave transformation presented in Eq. (2). Employing the balancing method between the second derivative term U'' and the cubic term U^3 in Eq. (13), we determine the balancing number $N = 1$. Substituting this result into Eq. (4), we proceed to construct the soliton solutions explicitly, laying the further analysis of their dynamical properties.

$$U(\xi) = \Lambda_0\ + \Lambda_1\ \mathfrak{U}(\xi). \tag{14}$$

Assume that $\mathfrak{U}(\xi)$ is the solution of the ODE:

$$\mathfrak{U}'(\xi) = ln(v)(b_1 + b_2\mathfrak{U}(\xi) + b_3\mathfrak{U}^2(\xi)) \tag{15}$$

By substituting Eqs. (15) and (14) into Eq. (13), we obtain a nonlinear algebraic system by setting the coefficients of identical powers of $\mathfrak{U}(\xi)$ to zero.

$$
\begin{aligned}
&\mathfrak{U}^{0J}(\xi) : \Lambda_1 b_2\, b_1\ (\ln(v))^2 + \beta\, {\Lambda_0}^3 + \Lambda_0 \lambda = 0,\\
&\mathfrak{U}^{1J}(\xi) : 3\,\beta\, {\Lambda_0}^2 \Lambda_1 + \Lambda_1 \lambda + \Lambda_1 \left(2\ (\ln(v))^2\, b_3\, b_1 + (\ln(v))^2\, {b_2}^2\right) = 0,\\
&\mathfrak{U}^{2J}(\xi) : 3\,\Lambda_1 b_2\ (\ln(v))^2\, b_3 + 3\,\beta\,\Lambda_0 {\Lambda_1}^2 = 0,\\
&\mathfrak{U}^{3J}(\xi) : 2\,\Lambda_1\,(\ln(v))^2\, {b_3}^2 + \beta {\Lambda_1}^3 = 0.
\end{aligned}
\tag{16}
$$

Different sets of solutions were obtained by solving the system of algebraic equations using Maple. From these solutions, we derived the explicit form of the solution to the problem as follows:

$$
\Lambda_0 = \sqrt{\frac{-(2\ln(v)^2 b_3 b_1 + 2)}{\beta}}, \quad \Lambda_1 = \sqrt{\frac{-2}{\beta}} b_3 \ln(v), \quad b_2 = -\frac{\sqrt{\frac{-2}{\beta}}\beta\sqrt{\frac{-(2\ln(v)^2 b_3 b_1 + 2)}{\beta}}}{\ln(v)}
\tag{17}
$$

The system of algebraic equations solved using Maple, which gave several sets of soliton solutions. From these results, we subsequently derived the explicit analytical form of the equation's solution as follows:

Case 1: If $\Delta < 0$ and $b_3 \neq 0$,

$$
\begin{aligned}
u_1(x,y,t) &= \frac{e^{is} ln(v)}{\sqrt{-2\beta}} \left(-b_2 + \sqrt{-\Delta} tan_v(\frac{\sqrt{-\Delta}}{2}(\xi)\right) + \sqrt{\frac{-2ln(v)^2 b_3 b_1 + 2}{\beta}},\\
u_2(x,y,t) &= \frac{e^{is} ln(v)}{\sqrt{-2\beta}} \left(-b_2 - \sqrt{-\Delta} cot_v(\frac{\sqrt{-\Delta}}{2}(\xi)\right) + \sqrt{\frac{-2ln(v)^2 b_3 b_1 + 2}{\beta}},\\
u_3(x,y,t) &= \frac{e^{is} ln(v)}{\sqrt{-2\beta}} \left(-b_2 - \sqrt{-\Delta}\left(tan_v(\sqrt{-\Delta}\xi) \pm i\sqrt{rs} sec_v(\sqrt{-\Delta}\xi)\right)\right) + \sqrt{\frac{-2ln(v)^2 b_3 b_1 + 2}{\beta}},\\
u_4(x,y,t) &= \frac{e^{is} ln(v)}{\sqrt{-2\beta}} \left(-b_2 - \sqrt{-\Delta}\left(cot_v(\sqrt{-\Delta}\xi) \pm \sqrt{rs} csc_v(\sqrt{-\Delta}\xi)\right)\right) + \sqrt{\frac{-2ln(v)^2 b_3 b_1 + 2}{\beta}},\\
u_5(x,y,t) &= \frac{e^{is} ln(v)}{\sqrt{-2\beta}} \left(-b_2 - \frac{\sqrt{-\Delta}}{2}\left(tan_v(\frac{\sqrt{-\Delta}}{4}\xi) - cot_v(\frac{\sqrt{-\Delta}}{4}\xi)\right)\right) + \sqrt{\frac{-2ln(v)^2 b_3 b_1 + 2}{\beta}},
\end{aligned}
\tag{18}
$$

Case 2: If $\Delta > 0$ and $b_3 \neq 0$,

$$
\begin{aligned}
u_6(x,y,t) &= \frac{e^{is} ln(v)}{\sqrt{-2\beta}} \left(-b_2 + \sqrt{\Delta} tanh_v(\frac{\sqrt{\Delta}}{2}(\xi)\right) + \sqrt{\frac{-2ln(v)^2 b_3 b_1 + 2}{\beta}},\\
u_7(x,y,t) &= \frac{e^{is} ln(v)}{\sqrt{-2\beta}} \left(-b_2 + \sqrt{\Delta} coth_v(\frac{\sqrt{\Delta}}{2}(\xi)\right) + \sqrt{\frac{-2ln(v)^2 b_3 b_1 + 2}{\beta}},\\
u_8(x,y,t) &= \frac{e^{is} ln(v)}{\sqrt{-2\beta}} \left(-b_2 + \sqrt{\Delta}\left(tanh_v(\sqrt{\Delta}\xi) \pm i\sqrt{rs} sech_v(\sqrt{\Delta}\xi)\right)\right) + \sqrt{\frac{-2ln(v)^2 b_3 b_1 + 2}{\beta}},\\
u_9(x,y,t) &= \frac{e^{is} ln(v)}{\sqrt{-2\beta}} \left(-b_2 + \sqrt{\Delta}\left(coth_v(\sqrt{\Delta}\xi) \pm \sqrt{rs} csch_v(\sqrt{\Delta}\xi)\right)\right) + \sqrt{\frac{-2ln(v)^2 b_3 b_1 + 2}{\beta}},\\
u_{10}(x,y,t) &= \frac{e^{is} ln(v)}{\sqrt{-2\beta}} \left(-b_2 - \frac{\sqrt{\Delta}}{2}\left(tanh_v(\frac{\sqrt{\Delta}}{4}\xi) + coth_v(\frac{\sqrt{\Delta}}{4}\xi)\right)\right) + \sqrt{\frac{-2ln(v)^2 b_3 b_1 + 2}{\beta}},
\end{aligned}
\tag{19}
$$

Case 3: If $b_3 b_1 > 0$ and $b_2 = 0$,

$$u_{11}(x,y,t)=\frac{2e^{is}ln(v)}{\sqrt{-2\beta}}\left(\sqrt{b_1b_3}tan_v(\sqrt{b_1b_3}\xi)\right)+\sqrt{\frac{-2ln(v)^2b_3b_1+2}{\beta}},$$

$$u_{12}(x,y,t)=-\frac{2e^{is}ln(v)}{\sqrt{-2\beta}}\left(\sqrt{b_1b_3}cot_v(\sqrt{b_1b_3}\xi)\right)+\sqrt{\frac{-2ln(v)^2b_3b_1+2}{\beta}},$$

$$u_{13}(x,y,t)=\frac{2e^{is}ln(v)}{\sqrt{-2\beta}}\left(\sqrt{b_1b_3}\left(tan_v(2\sqrt{b_1b_3}\xi)+\sqrt{rs}\ \ sec_v(2\sqrt{b_1b_3}\xi)\right)\right)+\sqrt{\frac{-2ln(v)^2b_3b_1+2}{\beta}}, \tag{20}$$

$$u_{14}(x,y,t)=\frac{2e^{is}ln(v)}{\sqrt{-2\beta}}\left(\sqrt{b_1b_3}(-\cot_v(2\sqrt{b_1\,b_3}\xi)+\sqrt{rs}\csc_v(2\sqrt{b_1\,b_3}\xi)\right)+\sqrt{\frac{-2ln(v)^2b_3b_1+2}{\beta}},$$

$$u_{15}(x,y,t)=\frac{e^{is}ln(v)}{\sqrt{-2\beta}}\left(\sqrt{b_1b_3}\left(tan_v(\frac{\sqrt{b_1b_3}}{2}\xi)-cot_v(\frac{\sqrt{b_1b_3}}{2}\xi)\right)\right)+\sqrt{\frac{-2ln(v)^2b_3b_1+2}{\beta}},$$

Case 4: If $b_3b_1<0$ and $b_2=0$,

$$u_{16}(x,y,t)=-\frac{2e^{is}ln(v)}{\sqrt{-2\beta}}\left(\sqrt{-b_1b_3}tanh_v(\sqrt{-b_1b_3}\xi)\right)+\sqrt{\frac{-2ln(v)^2b_3b_1+2}{\beta}},$$

$$u_{17}(x,y,t)=-\frac{2e^{is}ln(v)}{\sqrt{-2\beta}}\left(\sqrt{-b_1b_3}coth_v(\sqrt{-b_1b_3}\xi)\right)+\sqrt{\frac{-2ln(v)^2b_3b_1+2}{\beta}},$$

$$u_{18}(x,y,t)=-\frac{2e^{is}ln(v)}{\sqrt{-2\beta}}\left(\sqrt{-b_1b_3}\left(tanh_v(2\sqrt{-b_1b_3}\xi)+\sqrt{rs}\ \ sech_v(2\sqrt{-b_1b_3}\xi)\right)\right)+\sqrt{\frac{-2ln(v)^2b_3b_1+2}{\beta}}, \tag{21}$$

$$u_{19}(x,y,t)=-\frac{2e^{is}ln(v)}{\sqrt{-2\beta}}\left(\sqrt{-b_1b_3}(coth_v(2\sqrt{-b_1\,b_3}\xi)+\sqrt{rs}csch_v(2\sqrt{-b_1\,b_3}\xi)\right)+\sqrt{\frac{-2ln(v)^2b_3b_1+2}{\beta}},$$

$$u_{20}(x,y,t)=-\frac{e^{is}ln(v)}{\sqrt{-2\beta}}\left(\sqrt{-b_1b_3}\left(tanh_v(\frac{\sqrt{-b_1b_3}}{2}\xi)+coth_v(\frac{\sqrt{-b_1b_3}}{2}\xi)\right)\right)+\sqrt{\frac{-2ln(v)^2b_3b_1+2}{\beta}},$$

Case 5: If $b_2=0$ and $b_3=b_1$ then,

$$u_{21}(x,y,t)=\frac{2e^{is}b_1ln(v)}{\sqrt{-2\beta}}\left(tan_v(b_1\xi)\right)+\sqrt{\frac{-2ln(v)^2b_1^2+2}{\beta}},$$

$$u_{22}(x,y,t)=-\frac{2e^{is}ln(v)b_1}{\sqrt{-2\beta}}\left(cot_v(b_1\xi)\right)+\sqrt{\frac{-2ln(v)^2b_1^2+2}{\beta}},$$

$$u_{23}(x,y,t)=\frac{2e^{is}ln(v)b_1}{\sqrt{-2\beta}}\left(tan_v(2b_1\xi)\pm\sqrt{rs}sec_v(2b_1\xi)\right)+\sqrt{\frac{-2ln(v)^2b_1^2+2}{\beta}}, \tag{22}$$

$$u_{24}(x,y,t)=\frac{2e^{is}ln(v)b_1}{\sqrt{-2\beta}}\left((-cot_v(2b_1\xi)\pm\sqrt{rs}csc_v(2b_1\xi))\right)+\sqrt{\frac{-2ln(v)^2b_1^2+2}{\beta}},$$

$$u_{25}(x,y,t)=\frac{e^{is}ln(v)b_1}{\sqrt{-2\beta}}\left(tan_v(\frac{b_1}{2}\xi)-cot_v(\frac{b_1}{2}\xi))\right)+\sqrt{\frac{-2ln(v)^2b_1^2+2}{\beta}},$$

Case 6: If $b_2 = 0$ and $b_3 = -b_1$ then,

$$u_{26}(x,y,t) = \frac{2e^{is}ln(v)b_1}{\sqrt{-2\beta}}\left(tanh_v(-b_1\xi)\right) + \sqrt{\frac{2ln(v)^2b_1^2+2}{\beta}},$$
$$u_{27}(x,y,t) = \frac{2e^{is}ln(v)b_1}{\sqrt{-2\beta}}\left(coth_v(-b_1\xi)\right) + \sqrt{\frac{2ln(v)^2b_1^2+2}{\beta}},$$
$$u_{28}(x,y,t) = -\frac{2e^{is}ln(v)b_1}{\sqrt{-2\beta}}\left(-tanh_v(-2b_1\xi) \pm i\sqrt{rs}sech_v(-2b_1\xi)\right) + \sqrt{\frac{2ln(v)^2b_1^2+2}{\beta}}, \tag{23}$$
$$u_{29}(x,y,t) = -\frac{2e^{is}ln(v)b_1}{\sqrt{-2\beta}}\left(-coth_v(-2b_1\xi) \pm \sqrt{rs}csch_v(-2b_1\xi)\right) + \sqrt{\frac{2ln(v)^2b_1^2+2}{\beta}},$$
$$u_{30}(x,y,t) = \frac{e^{is}ln(v)b_1}{\sqrt{-2\beta}}\left(tanh_v(\frac{-b_1}{2}\xi) + coth_v(\frac{-b_1}{2}\xi)\right) + \sqrt{\frac{2ln(v)^2b_1^2+2}{\beta}},$$

Case 7: If ${b_2}^2 = 4b_3b_1$ then,

$$u_{31}(x,y,t) = \left(\frac{-4e^{is}b_1b_3(b_2ln(v)\xi+2)}{b_2^2\xi\sqrt{-2\beta}}\right) + \sqrt{\frac{-2ln(v)^2b_3b_1+2}{\beta}}, \tag{24}$$

Case 8: If $b_2 = \lambda, b_1 = p\lambda (p \neq 0)$ and $b_3 = 0$ then,

$$u_{32}(x,y,t) = -\frac{2e^{is}ln(v)b_3}{\sqrt{-2\beta}}\left((v^{\lambda\xi}+p)\right) + \sqrt{\frac{-2ln(v)^2b_3b_1+2}{\beta}}, \tag{25}$$

Case 9: If $b_2 = b_3 = 0$ then,

$$u_{33}(x,y,t) = -\frac{2e^{is}ln(v)b_3}{\sqrt{-2\beta}}\left(b_1\xi ln(v)\right) + \sqrt{\frac{-2ln(v)^2b_3b_1+2}{\beta}}, \tag{26}$$

Case 10: If $b_2 = b_1 = 0$ then,

$$u_{34}(x,y,t) = -\frac{2e^{is}}{\sqrt{-2\beta}\xi} + \sqrt{\frac{-2ln(v)^2b_3b_1+2}{\beta}}, \tag{27}$$

Case 11: If $b_1 = 0$, and $b_2 \neq 0$ then,

$$u_{35}(x,y,t) = -\frac{2e^{is}ln(v)}{\sqrt{-2\beta}}\left(\frac{rb_2}{(cosh_v(b_3\xi) - sinh_v(b_3\xi)+r)}\right) + \sqrt{\frac{-2ln(v)^2b_3b_1+2}{\beta}},$$
$$u_{36}(x,y,t) = \frac{2e^{is}ln(v)}{\sqrt{-2\beta}}\left(\frac{-b_2(sinh_v(b_2\xi)+cosh_v(b_2\xi))}{(sinh_v(b_2\xi)+cosh_v(b_2\xi)+s)}\right) + \sqrt{\frac{-2ln(v)^2b_3b_1+2}{\beta}}, \tag{28}$$

Case 12: If $b_2 = \lambda, b_3 = p\lambda$ and $b_1 = 0$ then,

$$u_{37}(x,y,t) = \frac{2p\lambda e^{is}ln(v)}{\sqrt{-2\beta}}\left(\frac{v^{\lambda\xi}}{s-prv^{\lambda\xi}}\right) + \sqrt{\frac{-2ln(v)^2b_3b_1+2}{\beta}}. \tag{29}$$

4.1 Results and Discussion

This section analyzes the various derived solutions and evaluates the unique characteristics of the resulting physical structures. These methods improve our understanding of the influence on dynamic waves. The spatial variable (x) is represented by the horizontal axis, the time-dependent behavior (t) by the vertical axis and the depth axis by the amplitude (u). The pulse patterns are localized to the DSE. The waves retain their shape and do not ruin themselves after a time, a characteristic of soliton behavior and complex interference patterns are evident when the waves interact. This paper addresses the physical attribute of the model by showing 3D, 2D, and contour plot, which shows the outcome of the chosen parameter value. These graphical representations incorporate different soliton forms such as bright, dark and periodic based on hyperbolic, trigonometric and exponential forms of functions. In Fig. (1-a), plot the imaginary component of u_6 in a 3D graph which plots the periodic behavior in the surface (x, y, t). This plot reflects the soliton complex dynamics as it develops with time. The Fig. (1-b) displays a 2D plot of the periodic soliton, illustrating its structure along the x-axis at various times (t = 0.1,

0.3, and 0.5). In (c), the contour graph indicate regions of constant amplitude, allowing for the observation how the soliton wave behave over time in the (x,t) plan. In (d), the real part of u_6 shows the 3D dark soliton in the (x,y,t) plan. The figure (e) shown, 2D plot of the real part with time (t = 0.1, 0.2, and 0.3), and the figure (f) show the contour plot in the form of bright soliton. In Fig. (2-a), depict the 3D imaginary graph that illustrates the periodic soliton of u_7 in the (x,y,t) plane. Under the influence of noise, we can observe the soliton complex structure. (b) The 2D graphic depicts the soliton periodic behavior at (t = 0.1, 0.3, and 0.5), with each curve reflecting the profile at a specific time. In (c), the contour plot shown the soliton amplitude in the (x,t) plane. With constant amplitude, the contour lines show how noise modifies the soliton structure over time. In (d), the real part of u_7 illustrates the three-dimensional bright soliton in the (x,y,t) plane. The 2D plot of the bright soliton with different time curves is shown in (e), while the contour graph of the real part is shown in (f). In Fig. (3-a), we observe the 3D periodic wave of u_8 in the (x,y,t) plane. (b) The 2D graph displays the soliton periodic behavior, with each trajectory representing the graph at a specific time. In (c), contour plot illustrate how noise modifies the system's structure over time with areas of constant amplitude. The subfigure (d) displays the real part of u_8, which represents the 3D combination of bright and dark soliton, while the 2D graph of the combined soliton in the (x,t) plan is displayed in (e). The counter graph of the real part in the (x,t) plan is displayed in (f). In Fig. (4-a), we observe a 3D periodic wave of u_9, which reveals a complex structure with rapidly increasing amplitude. In Fig. (b), we see a 2D graph that illustrates the soliton behavior at (t=0.1,0.3 and 0.5). This graph indicates periodic behavior for the values of $x < -8$, followed by a rapid change or possible singularity closer to $x = -6$. In (c), we display the contour plot of the soliton amplitude in the (x,t) plane, where the contour lines illustrate the soliton structure over time. In (d), we display the real part of u_9 in a 3D bright soliton. The subfigure (e) shows the 2D graph in the (x,t) plan with time (t = 0.1, 0.3, and 0.5), while (f) shows the contour graph of the real part. Fig. (5-a) 3D periodic graphs offer a multifaceted view of the function $u_{31}(x,y,t)$, allowing for both a broad understanding of its overall behavior and a detailed analysis of specific features. The 3D graph provides an intuitive understanding of the function's evolution; (b) the 2D graphs allow for precise comparisons over time; and (c) the contour plot highlights critical patterns and interactions within the (x,t) plane. The subfigure (d) shows the bright soliton of the real part of u_{31} in the 3D plan with the 2D plot shown in (e) and the contour representation of the real part shown in (f). Fig. (6-a) shows the 3D periodic graphs offer a multifaceted view of the function $u_{35}(x,y,t)$, allowing for broad understanding of its overall behavior and a detailed analysis of specific features. (b) The 2D graphs allow for accurate comparisons over time, revealing the behavior of soliton at times (t=0.1, 0.3, and 0.5). (c) The contour plot identifies critical patterns and interactions within the (x,t) plane. In (d), we show the 3D graph of u_{35} in the (x,y,t) plan, and the 2D graph of the real part of u_{35} with different time is shown in (e). The contour representation of the real part of u_{35} is shown in (f). Fig. (7-a) shows a periodic 3D graph of u_{37} in the (x,y,t) plane. It depicts a structure whose amplitude rapidly increases when noise is present. (b) showcases a 2D graph that illustrates the soliton structure at time (t=0.1, 0.3 , and 0.5). Each curve on the graph represents a specific time profile. The graph shows a periodic wave before $x < -7$, followed by a sudden and significant change or potential singularity near $x = -6$, and after $x = -7$, the graph show again a periodic wave with high amplitude, which may alter its shape as t varies. The contour plot in figure (c) illustrates the soliton's amplitude in the (x,t) plane over time.

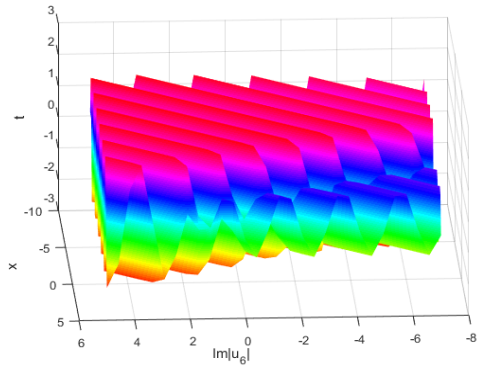

(a) 3D-Imaginary plot of u_6

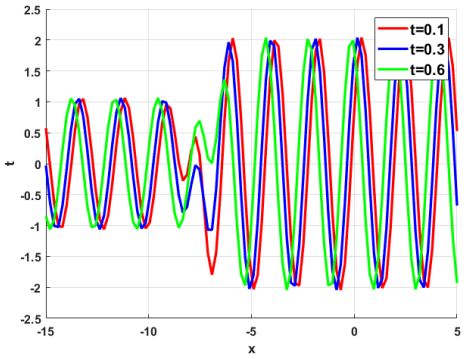

(b) 2D-Imaginary plot of u_6

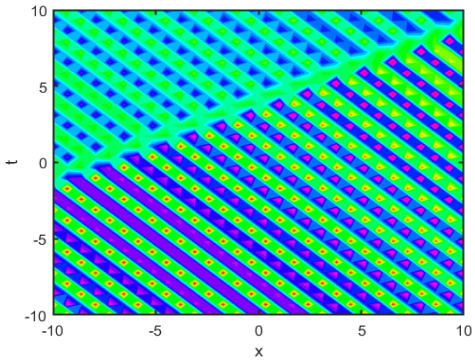

(c) contour-Imaginary plot of u_6

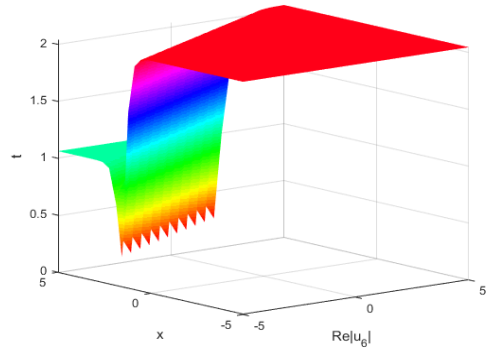

(d) 3D-Real plot of u_6

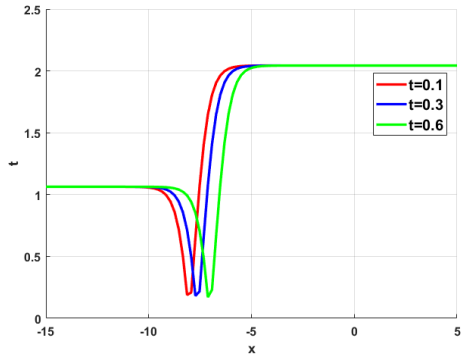

(e) 2D-Real plot of u_6

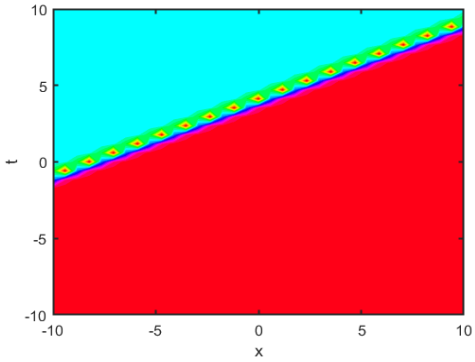

(f) Contour-Real plot of u_6

Figure 1: The periodic solution and dark soliton are illustrated in Fig. 1, where the imaginary part of the solution is shown in subfigures (a–c), and real part is depicted in subfigures (d–f), of $u_6(x, y, t)$ with parameter value $m = 1$, $y = 4$, $a = 2$, $g = 2$, $h = 2$, $f = 3$, $n = 2$ with (t=0.1, 0.3, 0.5).

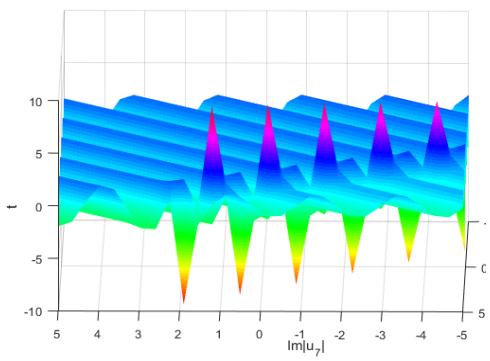

(a) 3D-Imaginary plot of u_7

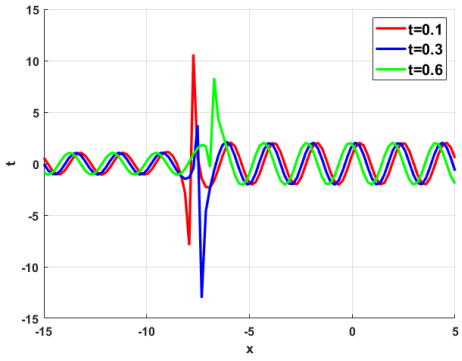

(b) 2D-Imaginary plot of u_7

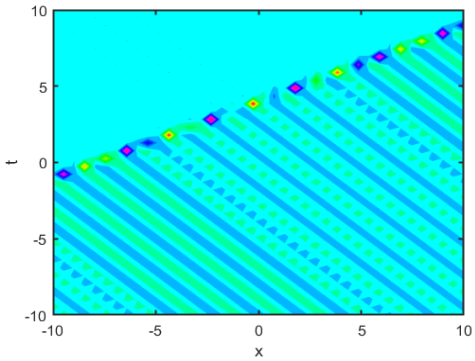

(c) Contour-Imaginary plot of u_7

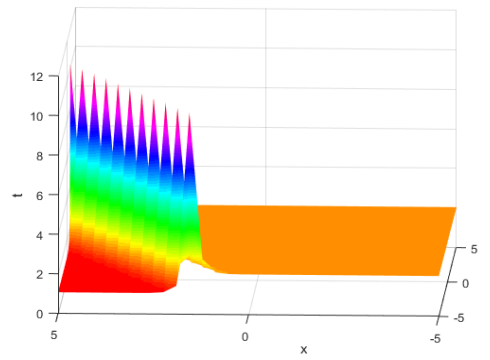

(d) 3D-Real plot of u_7

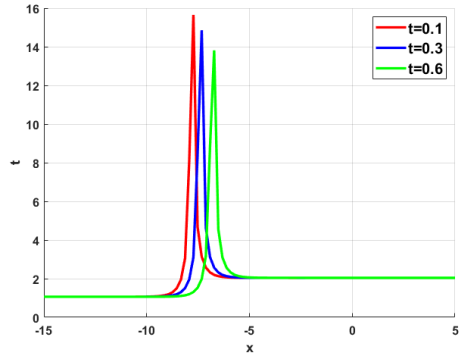

(e) 2D-Real plot of u_7

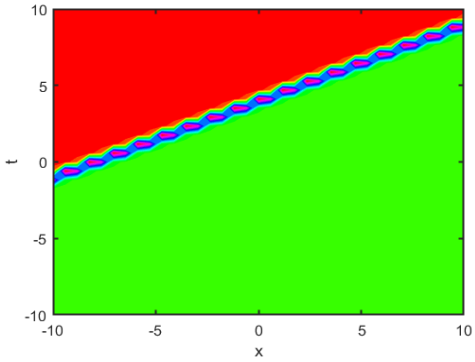

(f) Contour-Real plot of u_7

Figure 2: The periodic singular solution and dark soliton are illustrated in Fig. 2, where the imaginary part of the solution is shown in subfigures (a–c) and real part is depicted in subfigures (d–f), of $u_7(x, y, t)$ with parameter value $m = 1$, $y = 4$, $a = 2$, $g = 2$, $h = 2$, $f = 3$, $n = 2$ with (t=0.1, 0.3, 0.5).

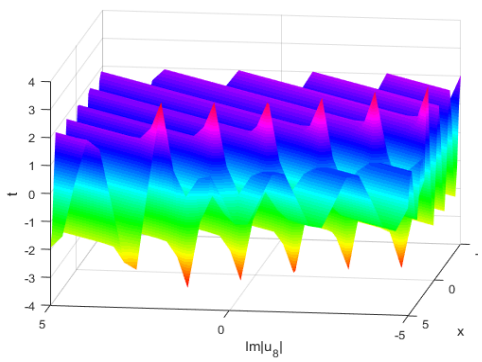

(a) 3D-Imaginary plot of u_8

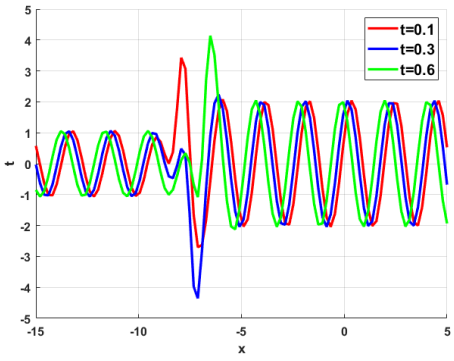

(b) 2D-Imaginary plot of u_8

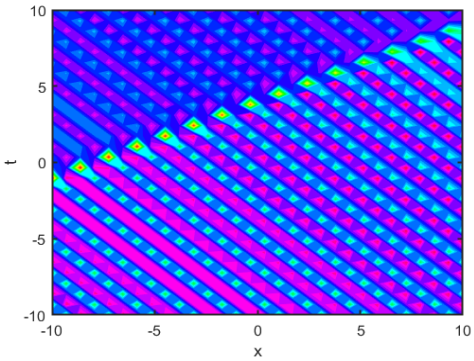

(c) Contour-Imaginary plot of u_8

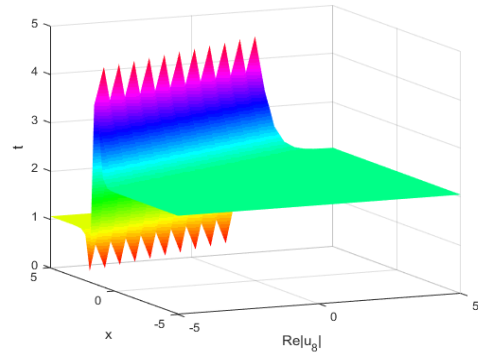

(d) 3D-Real plot of u_8

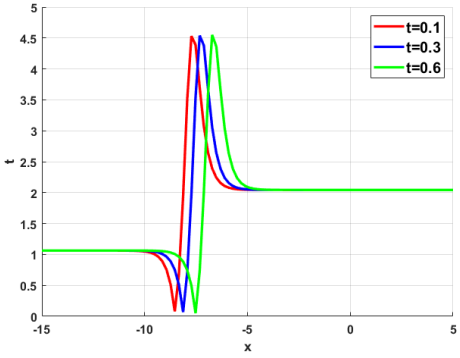

(e) 2D-Real plot of u_8

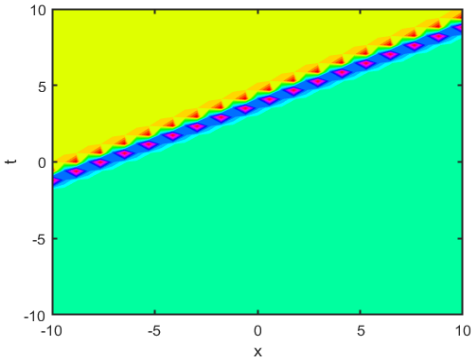

(f) Contour-Real plot of u_8

Figure 3: The periodic soliton and combination of bright and dark soliton are illustrated in Fig. 3, where the imaginary part of the solution is shown in subfigures (a–c) and real part is depicted in subfigures (d–f), of $u_8(x, y, t)$ with parameter value $m = 1$, $y = 4$, $a = 2$, $g = 2$, $h = 2$, $f = 3$, $n = 2$ with (t=0.1, 0.3, 0.5).

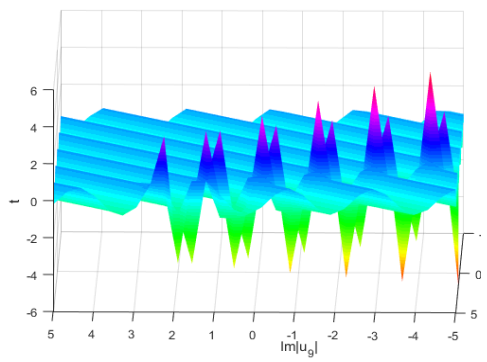

(a) 3D-Imaginary plot of u_9

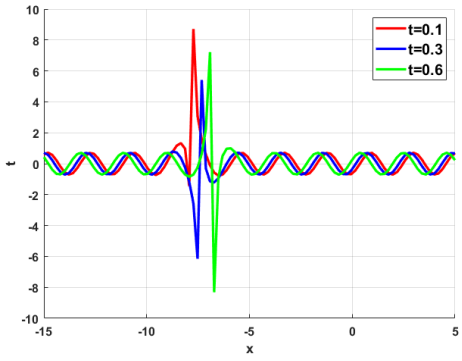

(b) 2D-Imaginary plot of u_9

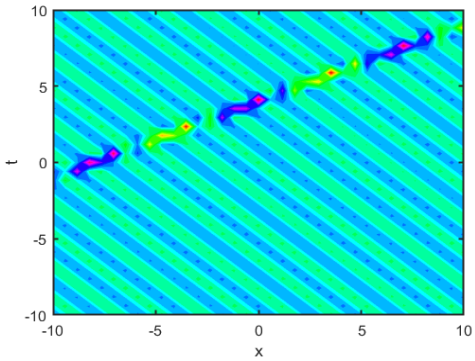

(c) Contour-Imaginary plot of u_9

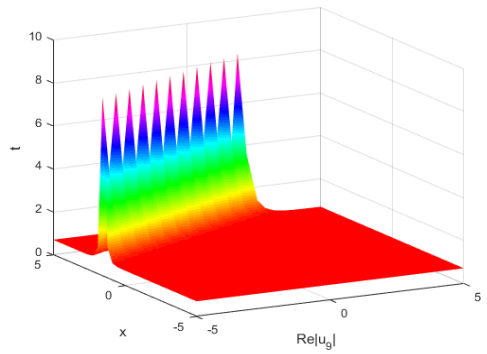

(d) 3D-Real plot of u_9

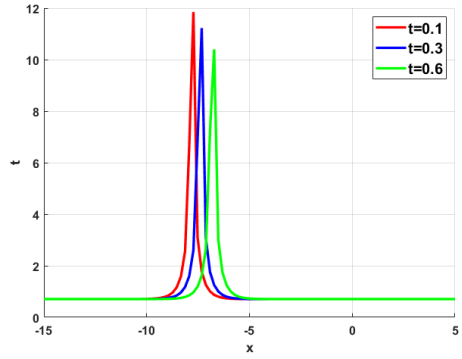

(e) 2D-Real plot of u_9

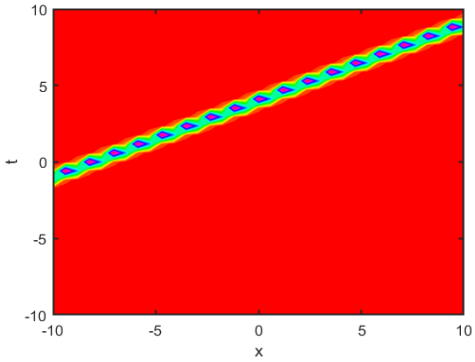

(f) Contour-Real plot of u_9

Figure 4: The periodic soliton and bright soliton are illustrated in Fig. 4, where the imaginary part of the solution is shown in subfigures (a–c) and real part is depicted in subfigures (d–f), of $u_9(x, y, t)$ with parameter value $m = 1$, $y = 4$, $a = 2$, $g = 2$, $h = 2$, $f = 3$, $n = 2$ with (t=0.1, 0.3, 0.5).

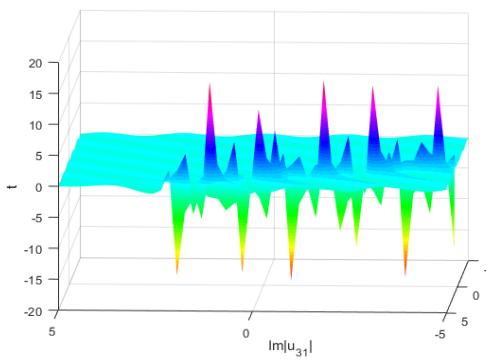

(a) 3D-Imaginary plot of $u_3 1$

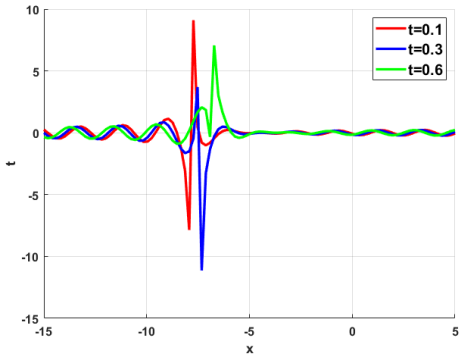

(b) 2D-Imaginary plot of $u_3 1$

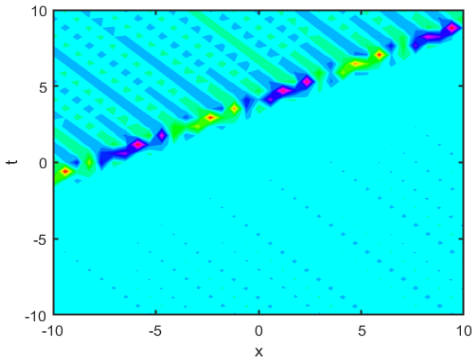

(c) Contour-Imaginary plot of $u_3 1$

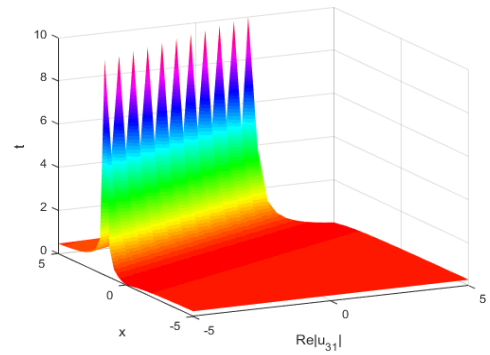

(d) 3D-Real plot of $u_3 1$

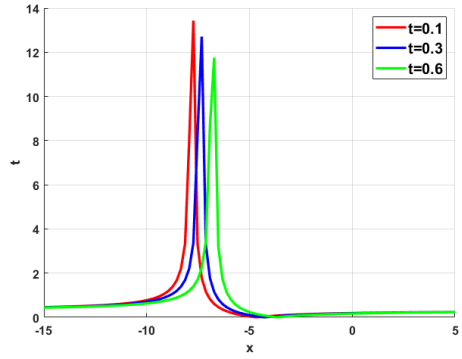

(e) 2D-Real plot of $u_3 1$

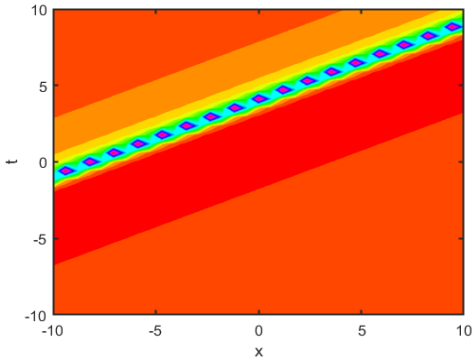

(f) Contour-Real plot of $u_3 1$

Figure 5: The periodic soliton and bright soliton are illustrated in Fig. 5, where the imaginary part of the solution is shown in subfigures (a–c) and real part is depicted in subfigures (d–f), of $u_{31}(x, y, t)$ with parameter value $m = 1$, $y = 4$, $a = 2$, $g = 2$, $h = 2$, $f = 3$, $n = 2$ with (t=0.1, 0.3, 0.5).

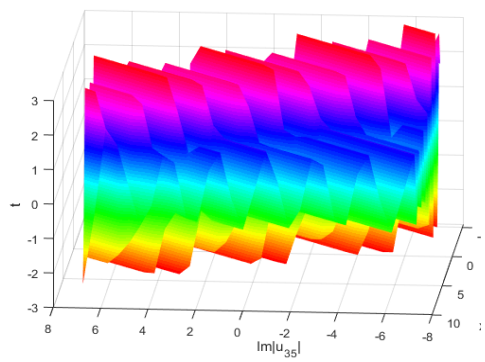

(a) 3D-Imaginary plot of $u_3 1$

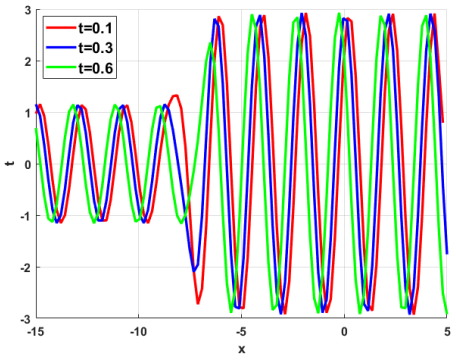

(b) 2D-Imaginary plot of $u_3 1$

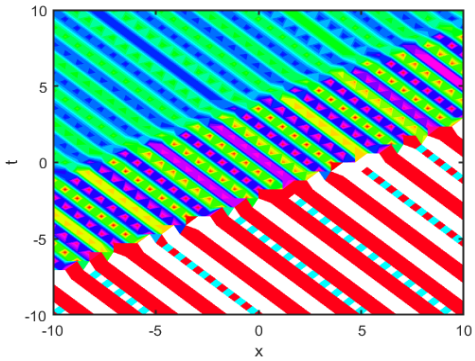

(c) Contour-Imaginary plot of $u_3 1$

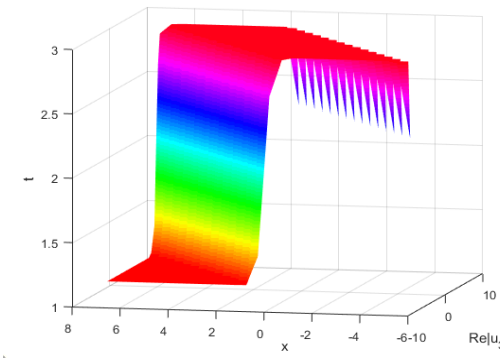

(d) 3D-Real plot of $u_3 5$

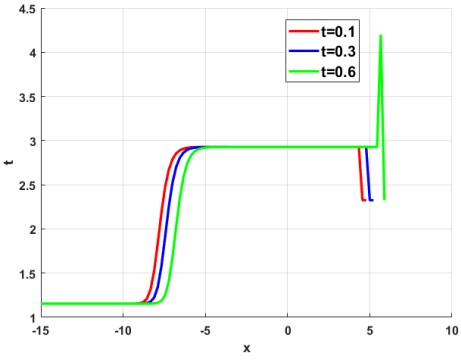

(e) 2D-Real plot of $u_3 5$

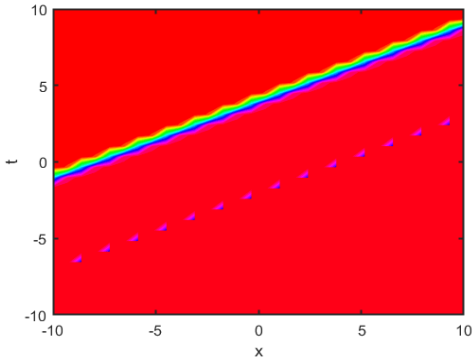

(f) Contour-Real plot of $u_3 5$

Figure 6: The periodic soliton and kink soliton are illustrated in Fig. 6, where the imaginary part of the solution is shown in subfigures (a–c) and real part is depicted in subfigures (d–f), of $u_{35}(x, y, t)$ with parameter value $m = 1$, $y = 4$, $a = 2$, $g = 2$, $h = 2$, $f = 3$, $n = 2$ with (t=0.1, 0.3, 0.5).

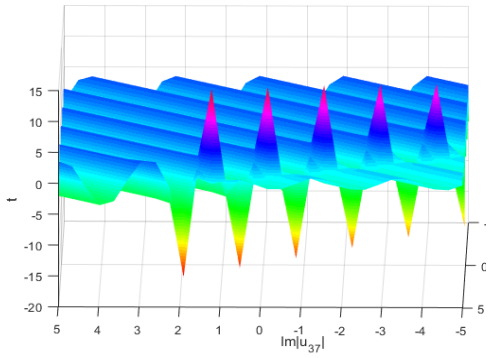

(a) 3D-Imaginary plot of $u_3 7$

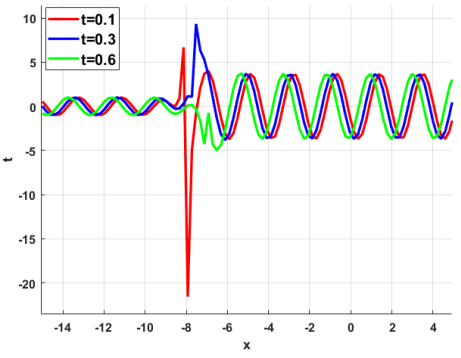

(b) 2D-Imaginary plot of $u_3 7$

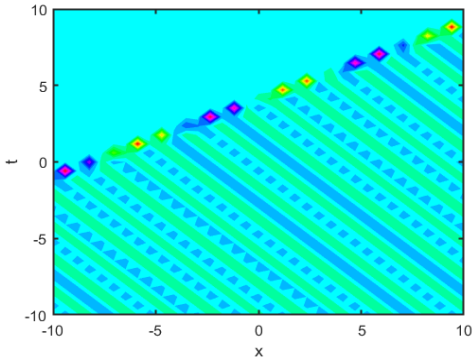

(c) Contour-Imaginary plot of $u_3 7$

Figure 7: The periodic solution are illustrated in Fig. 7, where the imaginary part of the solution is shown in subfigures (a–c) of $u_{37}(x, y, t)$ with parameter value $m = 1$, $y = 4$, $a = 2$, $g = 2$, $h = 2$, $f = 3$, $n = 2$ with (t=0.1, 0.3, 0.5).

5 Stability Analysis

To study the stability of Eq. (1), we examine the system's response to small disturbances about a steady base solution (u_0). We introduce a perturbation into Eq. (1), and retaining only first-order terms in $(\tilde{u})$. Yields the linearized model that governs the evolution of the perturbation and determines whether it grows or decays. Assume small perturbations about a steady base state (u_0, w_0):

$$u = u_0 + \tilde{u}, \qquad w = w_0 + \tilde{w}, \qquad |\tilde{u}|, |\tilde{w}| \ll 1 \tag{30}$$

Substituting into Eq. (1) gives

$$i(u_0 + \tilde{u})_t + \alpha_1(u_0 + \tilde{u})_{xx} + \alpha_2(w_0 + \tilde{w})(u_0 + \tilde{u}) = 0. \tag{31}$$

$$\alpha_3(w_0+\tilde{w})_y - \alpha_4\big(|u_0+\tilde{u}|^2\big)_x = 0. \tag{32}$$

Keeping only linear terms in $(\tilde{u},\tilde{w})$ and assuming u_0, w_0 are steady/uniform ($u_{0t}=0,\ u_{0xx}=0$), we obtain the linearized equation

$$i\,\tilde{u}_t + \alpha_1\tilde{u}_{xx} + \alpha_2(w_0\tilde{u} + u_0\tilde{w}) = 0. \tag{33}$$

$$\alpha_3\tilde{w}_y - 2\alpha_4 u_0\tilde{u}_x = 0. \tag{34}$$

Assume normal-mode perturbations:

$$\tilde{u} = u\,e^{i(fx+gy+ht)}, \qquad \tilde{w} = w\,e^{i(fx+gy+ht)}. \tag{35}$$

Substitute into Eq. (34) and Eq. (35):

$$i(ih)\tilde{u} + \alpha_1(-f^2)\tilde{u} + \alpha_2\big(w_0\tilde{u} + u_0\tilde{w}\big) = 0. \tag{36}$$

$$\alpha_3(ia)\tilde{w} - 2\alpha_4 u_0(if)\tilde{u} = 0 \tag{37}$$

Now to find the Value of $\tilde{w}$ and put in Eq. (38).

$$i\alpha_3 a\tilde{w} - 2\alpha_4 u_0 if\tilde{u} = 0 \tag{38}$$

$$\tilde{w} = \frac{2\alpha_4 u_0 f\tilde{u}}{\alpha_3 a}. \tag{39}$$

Plugging $\tilde{w}$ into the algebraic Eq. (37) gives

$$\tilde{u}(-h - \alpha_1 f^2 + \alpha_2 w_0 + \alpha_2 u_0(\frac{2\alpha_4 u_0 f\tilde{u}}{\alpha_3 a})) = 0. \tag{40}$$

For a nontrivial solution $\tilde{u} \neq 0$,

$$-h - \alpha_1 f^2 + \alpha_2 w_0 + \frac{2f\alpha_2\alpha_4 u_0^2}{a\alpha_3} = 0, \tag{41}$$

hence the dispersion relation is

$$h = -\alpha_1 f^2 + \alpha_2 w_0 + \frac{2f\alpha_2\alpha_4 u_0^2}{a\alpha_3}. \tag{42}$$

1. If $h > 0$, the perturbation grows exponentially, so the steady state is unstable.
2. If $h < 0$, the perturbation decays exponentially, so the steady state is stable.
3. If $h = 0$, the perturbation neither grows nor decays, indicating neutral (marginal) stability.

6 Dynamical Analysis

Several important techniques follow the qualitative time-dependent behavior of a system, providing the dynamical analysis of a model. Sensitivity analysis (SA), bifurcation analysis (BA), and chaos theory will be applied to determine the stability of the model with the use of different initial conditions. SA is used in determining the key parameters affect the system output with minimal changes. The phase diagram is a state-space diagram that plots state-space curves to show the patterns of fixed points, limit cycles, and chaotic attractors. In the case of models with multistability analysis (MA), a fixed set of parameters may support several stable states, and this is indicated by bifurcation diagrams. The Lyapunov exponent (LE) is the measurement of the sensitivity to the initial conditions, giving positive values in the case of chaotic systems and negative values in the case of stable systems. The Poincaré map shows continuous dynamics in a simplified form, and periodic orbits are easier to analyze, as well as assessed stability around fixed points. This goal is achieved by the use of these analytical tools to assist the proposed simulations and phase space reconstruction methods to assess the behavior of a system in terms of stability, periodicity, and complexity.

6.1 Phase Portrait Analysis

We examine the PP of the DS Fokas system, which develops in optical fiber under nonlinear propagation conditions, using the concepts of bifurcation theory. The planar dynamical system described by Eq. (13) is reformulated as follows:

$$\begin{cases} \frac{dU}{d\xi} & = P, \\ \frac{dP}{d\xi} & = -\lambda U(\xi) - \beta U^3(\xi). \end{cases} \tag{43}$$

Where $\lambda = \left(\frac{-f^2\alpha_1+h}{m^2\alpha_1}\right)$ and $\beta = \left(\frac{\alpha_2\alpha_4}{ma\alpha_1\alpha_3}\right)$. This system demonstrates Hamiltonian behavior and is characterized by the following fundamental properties.

$$G(U,P) = \frac{P^2}{2} + \lambda\frac{U^2}{2} + \beta\frac{U^4}{4} = g. \tag{44}$$

With g representing the Hamiltonian constant, we analyze the PP within the parameter space defined by λ and β for Eq. (44). By analyzing the dynamical system, we identify three equilibrium points: $M_1 = (0,0)$, $M_2 = (V_1,0)$, and $M_3 = (V_2,0)$ along the U-axis, where V_1 and V_2 are specified as follows.

$$V_1 = \sqrt{\frac{-\lambda}{\beta}}, V_2 = -\sqrt{\frac{-\lambda}{\beta}}. \tag{45}$$

The Jacobian matrix of the system is given by:

$$det\left(J(U,P)\right) = \begin{vmatrix} 0 & 1 \\ -\lambda - 3\beta U^2(\xi) & 0 \end{vmatrix} = \lambda + 3\beta U^2(\xi). \tag{46}$$

If $\det G(U,P) < 0$, the point is classified as a saddle, indicating a dynamic behavior where trajectories approach the equilibrium along some directions and diverge along others. If $\det G(U,P) > 0$, the point represents a center, where the system exhibits periodic behavior with trajectories forming closed orbits around the equilibrium. When $\det G(U,P) = 0$, the point is considered cuspidal, signifying a more complex and singular nature of the equilibrium, where the behavior may involve degenerate or more intricate dynamical features. The nature of these equilibrium points can be altered by adjusting the values of the system's parameters, offering a wide range of dynamical behaviors.

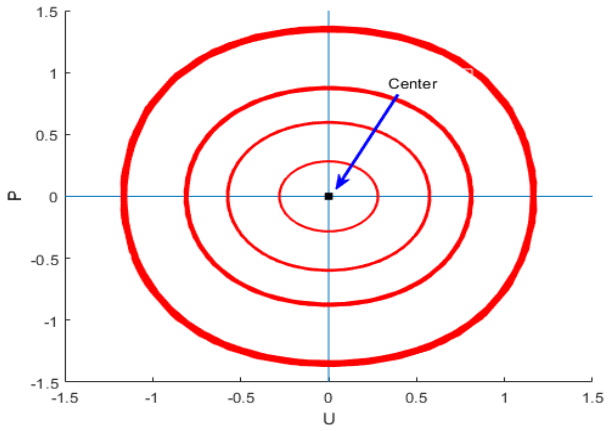

(a) $\lambda > 0$ and $\beta > 0$

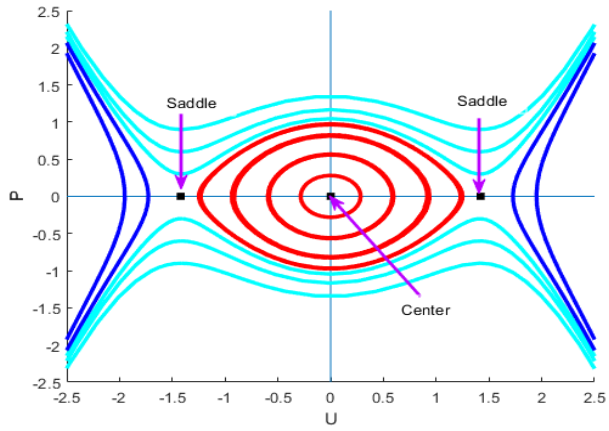

(b) $\lambda > 0$ and $\beta < 0$

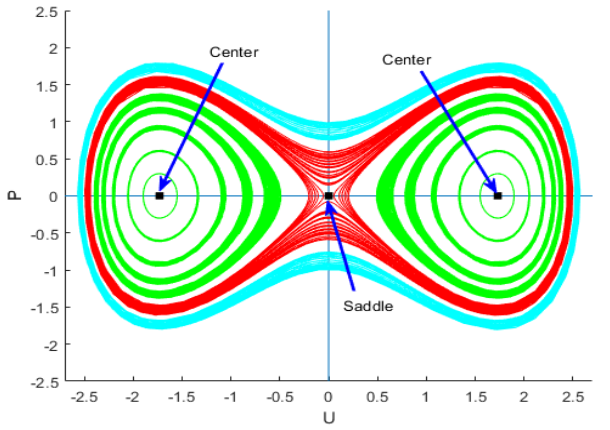

(c) $\lambda < 0$ and $\beta > 0$

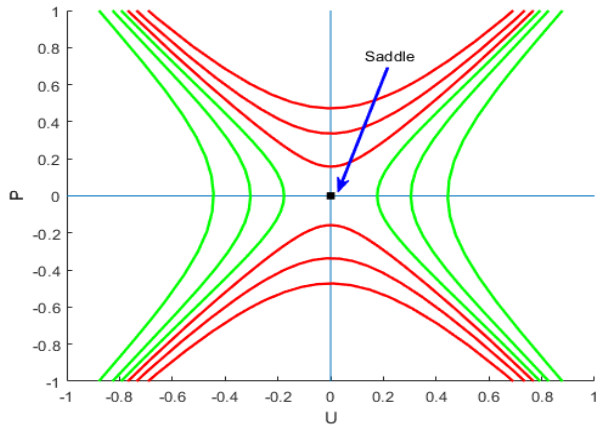

(d) $\lambda < 0$ and $\beta < 0$

Figure 8: PP analysis of the dynamical system

Case 1: In this case, $\lambda > 0$ and $\beta > 0$, we get three equilibrium point $M_1 = (0, 0)$, $M_2 = (i, 0)$ and $M_3 = (-i, 0)$ by using $\lambda = 1$ and $\beta = \frac{1}{2}$. Here we see in Fig. (8-a) M_1 represent the center point and M_2, M_3 imagenry point.
Case 2: In this case, $\lambda > 0$ and $\beta < 0$, we have three equilibrium point $M_1 = (0, 0)$, $M_2 = (1.42, 0)$ and $M_3 = (-1.42, 0)$ by using $\lambda = 1$ and $\beta = \frac{-1}{2}$. Here we see in Fig. (8-b) M_1 represent the center point and M_2, M_3 show the saddle point.
Case 3: In this case, $\lambda < 0$ and $\beta > 0$, we have three equilibrium point $M_1 = (0, 0)$, $M_2 = (1.73, 0)$ and $M_3 = (-1.73, 0)$ by using $\lambda = \frac{-3}{2}$ and $\beta = \frac{1}{2}$. Here we see in Fig. (8-c) that M_1 represents the saddle point and M_2, M_3 represents the center point.
Case 4: When $\lambda < 0$ and $\beta < 0$, we get three equilibrium point $M_1 = (0, 0)$, $M_2 = (i, 0)$ and $M_3 = (-i, 0)$ by using $\lambda = \frac{-3}{2}$ and $\beta = \frac{-1}{2}$. Here we see in Fig. (8-d) M_1 represent the Saddle point and M_2, M_3 imaginary point.

6.2 Sensitivity Analysis

Sensitivity analysis of the planar dynamical system is researched in numerous disciplines such as economics, optics, physics, engineering, mathematics, and the sciences to understand the impact of variation in input parameters on the model output. The procedure involves systematically modifying the value of the input parameters to observe the behavior of the dynamical system. This method supports informed decision making, process optimization, and risk assessment. It is essential to understand the complex structure of the systems, allowing for more accurate predictions and better control over outcomes.

SA of the proposed dynamical model was evaluated using the set of distinct initial conditions. The green trajectory represents the initial values $(U, P) = (0.1, 0)$. The blue curve corresponds to the second initial set $(U, P) = (0.16, 0)$, while the red curve illustrates the third initial condition, $(U, P) = (0.24, 0)$. Fig. 9(a–c) exhibits sensitivity during the transient time period and responds differently to the various initial conditions. Fig. (9-d) highlights this sensitivity in response to a slight modification in the initial state. These results confirm that even small changes in the initial conditions have a significant impact on the behavior of a dynamical system. Overall, the proposed model exhibits moderate sensitivity, without being excessively sensitive.

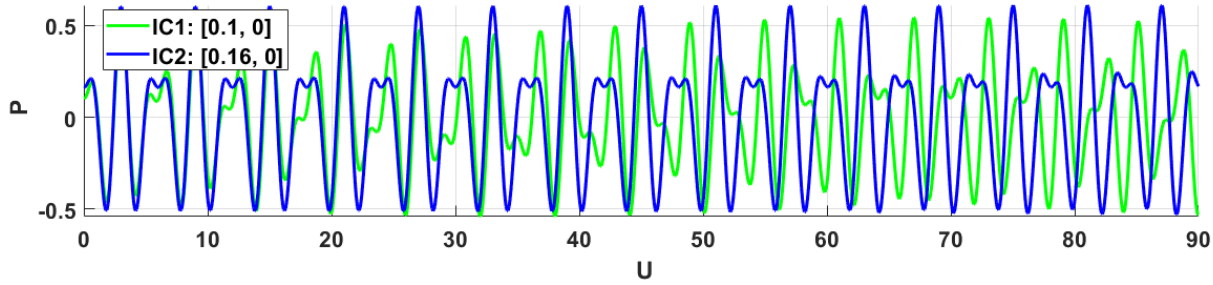

(a) (0.1,0) green, (0.16,0) blue

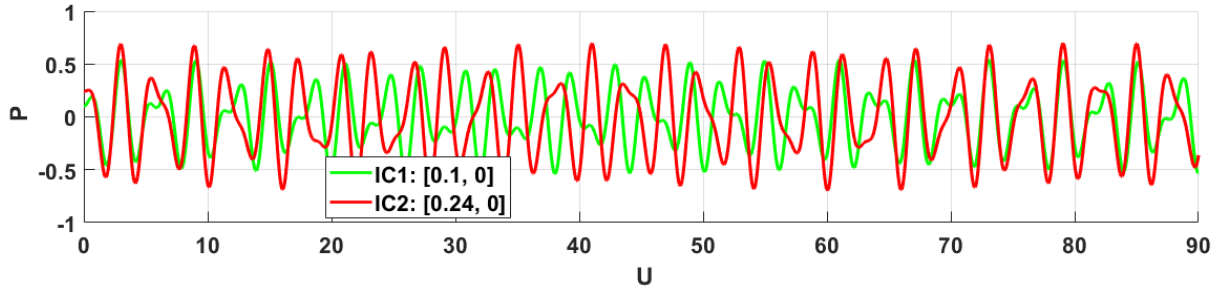

(b) (0.1,0) green, (0.24,0) red

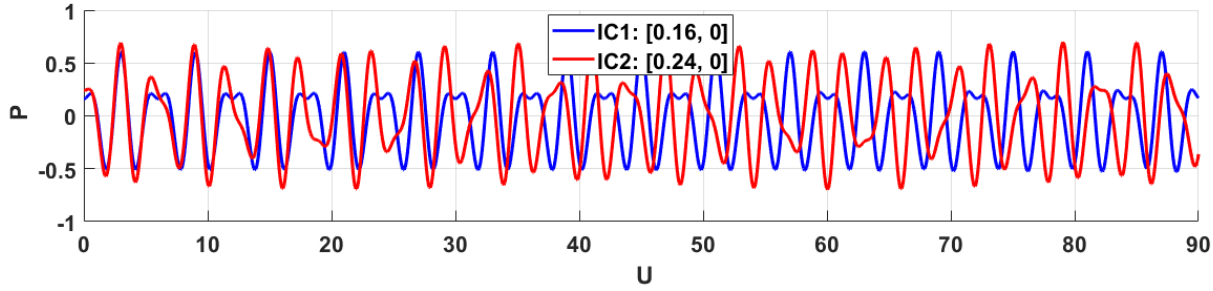

(c) (0.16,0) blue, (0.24,0) red

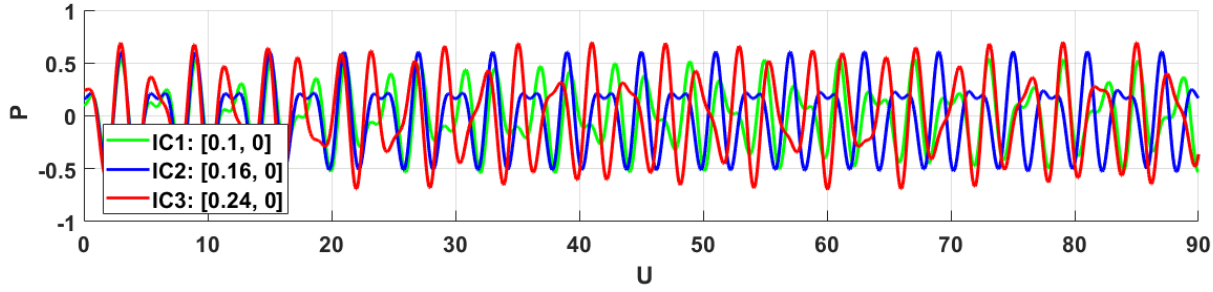

(d) (0.1,0) green, (0.16,0) blue, (0.24,0) red

Figure 9: Sensitivity analysis systems (44) using different initial conditions

6.3 Chaotic Analysis

This section discusses the random behavior of the proposed model. To analyze complex patterns more effectively add an external force $\varepsilon\cos(\alpha\xi)$ to the dynamical system (43), thereby allowing for a study of the effect of variation of this force on the dynamics of the system. The symbol ε is used to denote the intensity, while α represents the frequency of the perturbed component. These parameters play a crucial role in characterizing the behavior and influence of the perturbation on the system dynamics. Consequently, we can depict the enhanced system as the following:

$$\begin{cases} \frac{dU}{d\xi} & = P, \\ \frac{dP}{d\xi} & = -\lambda U(\xi) - \beta U^3(\xi) + \varepsilon cos(F), \\ \frac{dE}{d\xi} & = \alpha. \end{cases} \tag{47}$$

Where $F = \alpha\xi$. We examine the chaotic behavior of the dynamical system (47) to apply different external forces. Assess

the dynamic behavior of the perturbed system, to evaluate a range of arbitrary values for the physical parameters. Examine the effects of varying parameters value ϵ, λ, β and α. This analysis helps us to understand how changes in these parameters influence the system's behavior and dynamics, providing insights into their relative importance and the sensitivity of the system to their variations.

•Fig. 10, presents 3D and 2D phase plots with time series graphs at the initial values $\epsilon = 0.03$, $\alpha = 0.1$, $\lambda = 1.7$, and $\beta = -0.4$. In this scenario, where the external force has minimal intensity and frequency, the system described by equation (35) exhibits periodic behavior, demonstrating a stable and repeating pattern in its dynamics.

• Fig. 11, displays visual representations through 3D, 2D, and time series plots. We perform a time analysis at the parameter values $\epsilon = 0.3$, $\alpha = \pi$, $\lambda = 3.7$, and $\beta = -0.6$. Eq. (44) describes the system's quasi-periodic behavior, which undergoes notable changes as the intensity and frequency of the external force increase, indicating a transition in its dynamic pattern.

• Fig. 12, illustrates the behavior of the system when increasing the amplitude and also frequency with $\epsilon = 0.9$ and $\alpha = 2\pi$, dynamical system exibit the chaotic behavior in the system as described by system (44). This figure highlights how significant changes in these parameters influence the system's dynamics, leading to more complex and unpredictable behavior.

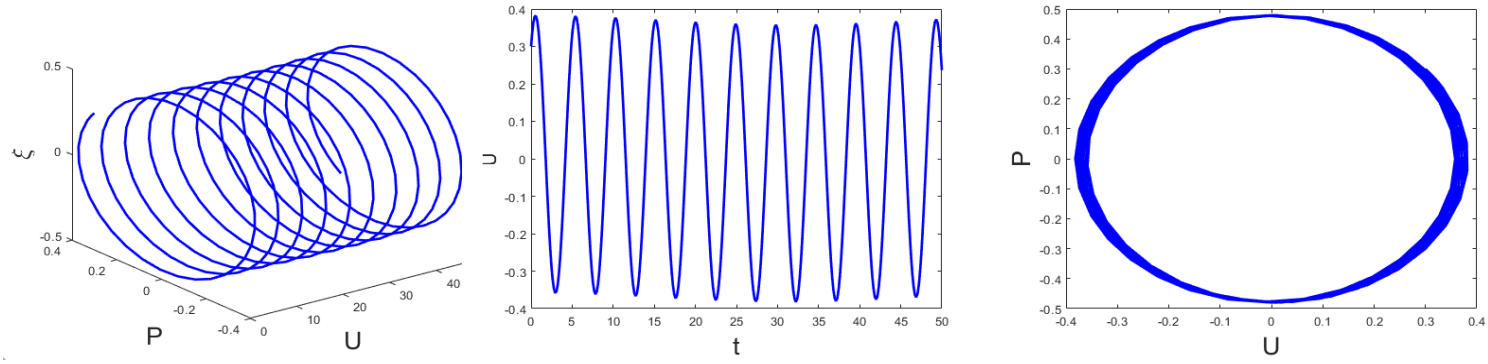

(a) 3D-Phase profile (b) Time series (c) 2D-Phase profile

Figure 10: Periodic behavior within systems (44)

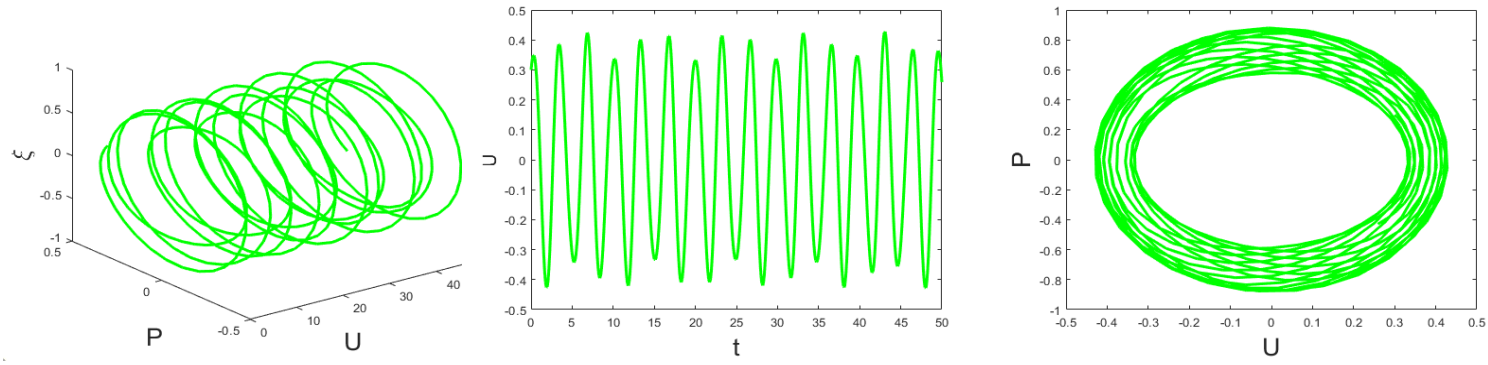

(a) 3D-Phase profile (b) Time series (c) 2D-Phase profile

Figure 11: Quasi-periodic patterns within systems (44)

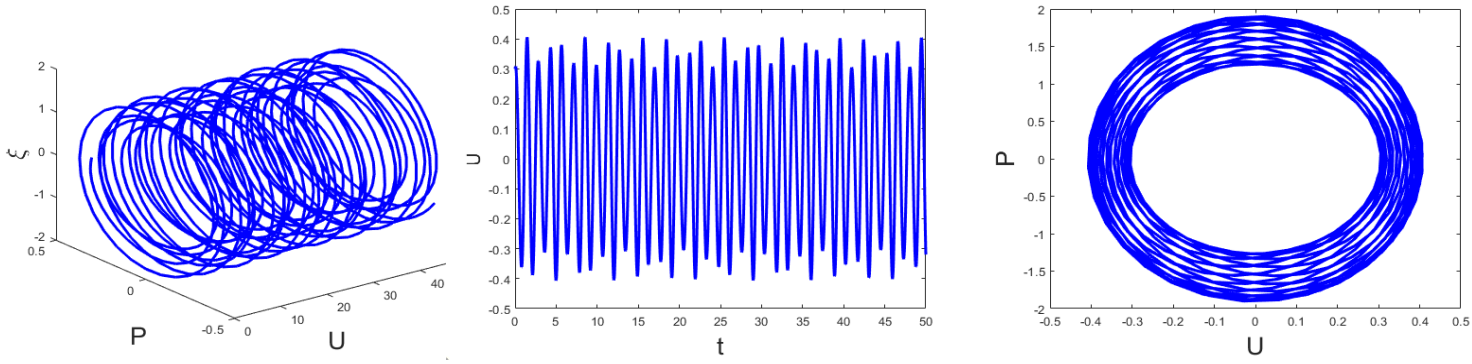

(a) 3D-Phase profile (b) Time series (c) 2D-Phase profile

Figure 12: Chaotic behavior within systems (44)

6.4 Lyapunove Exponent

LE used to describe the rate of separation of closed trajectories in a dynamical system. These exponents assist in establishing the stability of a given system and the predictability of its future. In chaos theory, a positive LE implies the presence of a sensitive dependence on initial conditions, whereas a negative LE indicates convergence, which is a measure of the stability of a system. Besides, the LE grow with the dimensionality of the system, and thus higher dimensional systems are more complicated. Each of the exponents plays a role in defining the system as periodic, quasi-periodic, or chaotic. Although all LE are informative, the most important one is the largest one, and the sign of the LE gives information on whether the system is chaotic or not. LE have extensive uses in many aspects of physics, engineering, and applied mathematics, in particular the study of dynamical systems and other nonlinear structures.

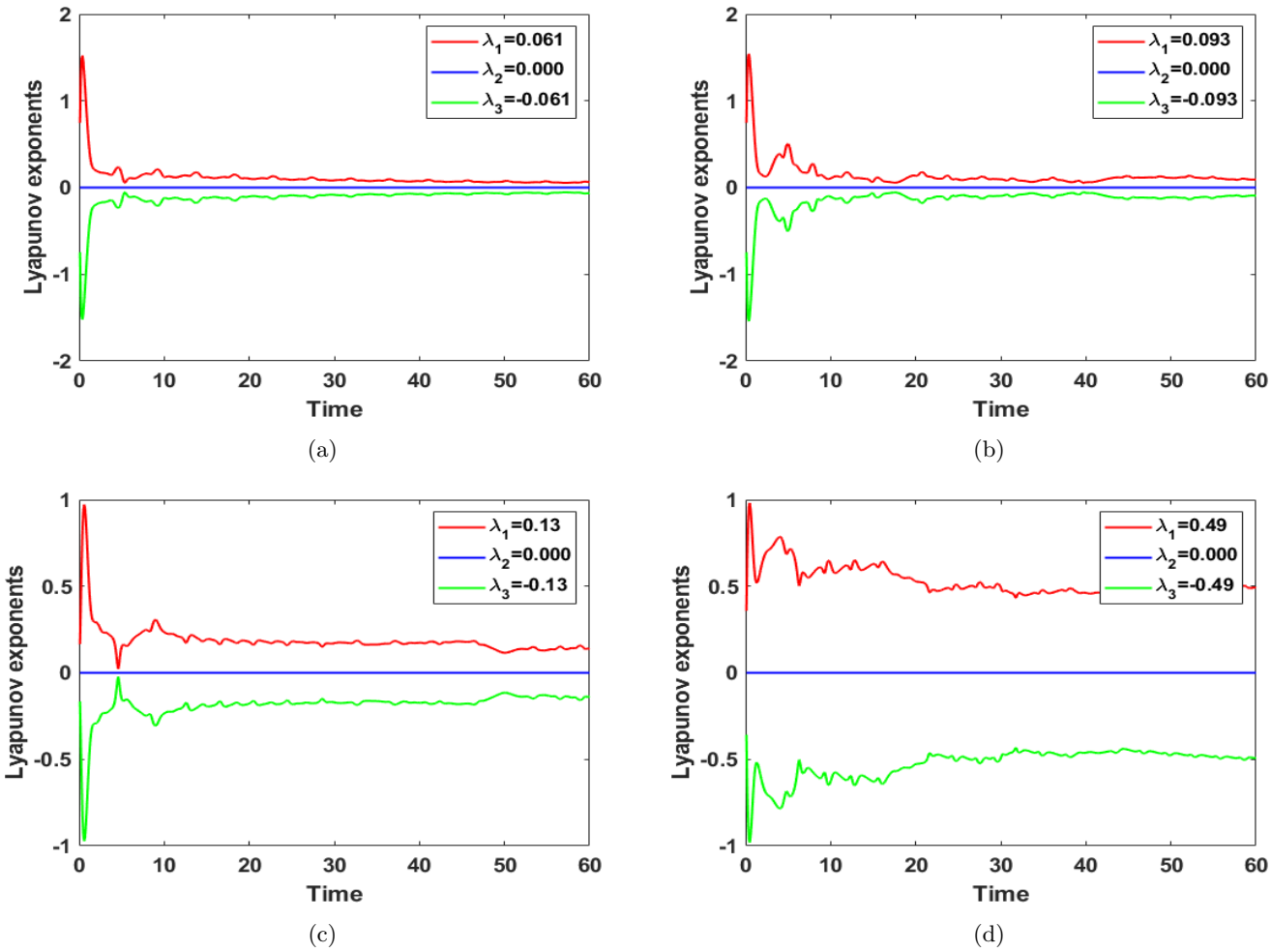

Figure 13: The Lyapunov exponent changes with the system parameter, showing the change from stable (negative exponent) to chaotic (positive exponent) states of the systems (44)

6.5 Multistability

The phenomenon of multistability is such that a given dynamical system exhibits the capacity to possess several stable states or attractors that all coexist simultaneously under the same parameters. With the passage of time, the system is bound to develop into a wide range of long-term behaviors that can express themselves as fixed points, periodic orbits, or even as chaotic attractors, depending to a large degree on the specific initial conditions under which the system starts to evolve. The phenomenon is typically seen in nonlinear systems, and it is of very great importance in a vast field of study, including but not limited to biology, physics, engineering, and neuroscience. A range of complex behavior is possible due to multistability, especially behavior like state transitions in an abrupt manner that is provoked by even very slight variations in the system's parameters or initial conditions. It is very crucial to have complete knowledge of multistability for effective control of the system's behavior and prediction of how the system will react, especially in applications of utmost importance involving memory storage, pattern recognition, and decision-making mechanisms.

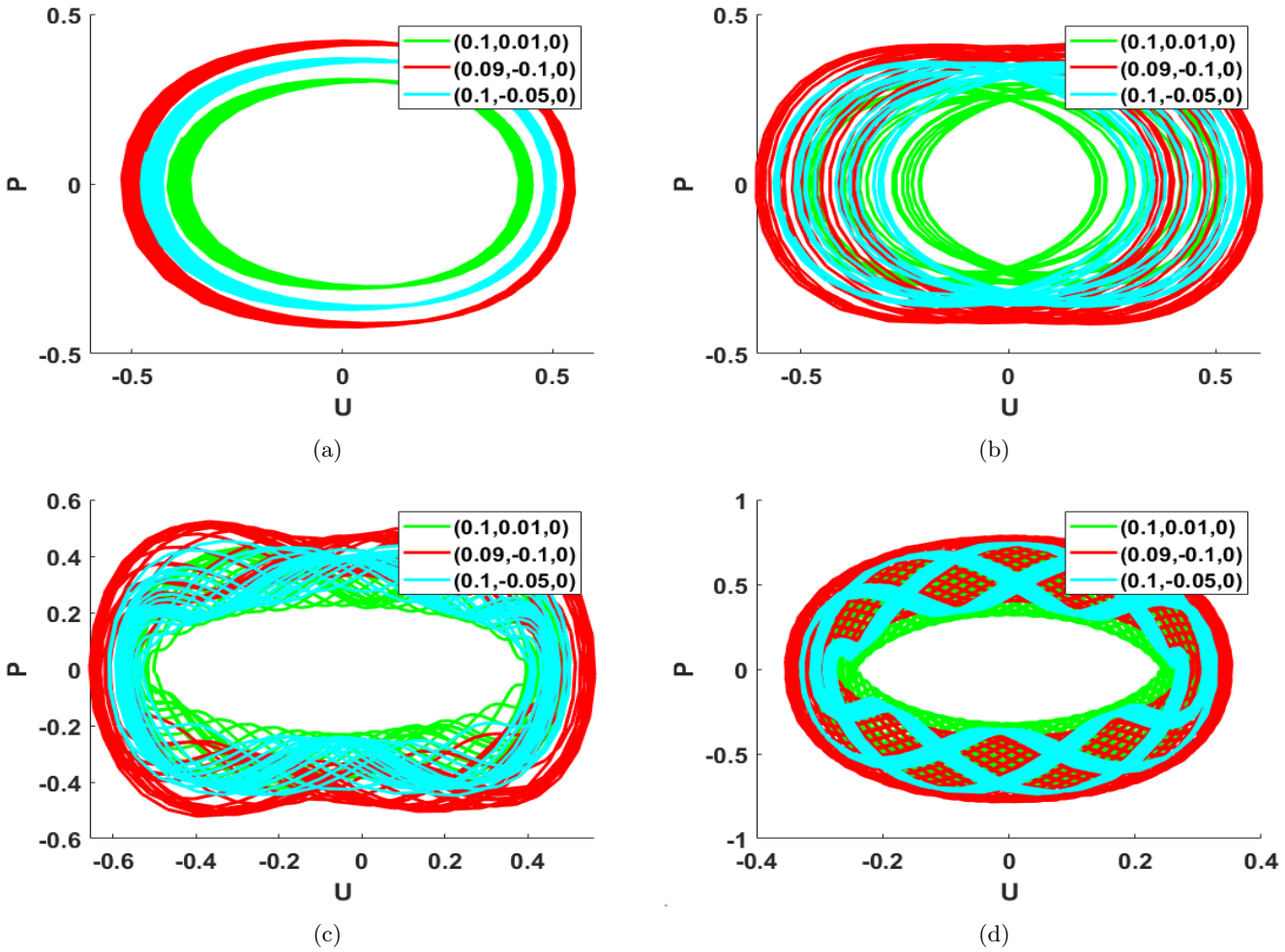

Figure 14: Illustration of multistability in the system, showcasing the existence of multiple coexisting stable attractors under identical parameter values, with system evolution exhibiting significant sensitivity to initial conditions of the systems (44)

7 Conclusion

In this paper, we examine the wave structure of the DS Fokas system by using the MKM, which enhances our understanding of nonlinear phenomena especially in optical fibers. A wide variety of soliton profiles were systematically constructed, including bright, anti-kink, dark and periodic type, to demonstrate the robustness and applicability of the proposed model. We used MATLAB to plots the graphical behavior using carefully selected parameter values, to reveal the diverse behaviors and complex dynamics inherent in Figs. (1-7). The solutions obtained are of various types, including hyperbolic, trigonometric, exponential functions, and rational expressions. By presenting a broad spectrum of solutions, we highlight the model's capability to effectively describe complex nonlinear phenomena. This detailed treatment not only reinforces the theoretical framework but also delineates its potential applications in advancing the study of soliton dynamics and related fields. Additionally, we investigated the dynamical analysis of the nonlinear DS Fokas system using the principles of bifurcation theory. Fig. (8) shows the phase portrait of the proposed system with different initial conditions. Fig. (9) illustrate the sensitivity of dynamical systems using the Runge-Kutta method, highlighting the response of the DS Fokas system to minor variations in initial conditions. We illustrate the chaotic behavior of the planar dynamical system by introducing an external force and analyzing whether the system exhibits periodic or chaotic behavior as the external force varies. When a small external force is applied, the system remains in its original state and displays periodic behavior. As the external force increases, the system shows some disturbance but eventually returns to its original state, which is referred to as quasi-periodic behavior. In the quasi-periodic state, the system exhibits periodic patterns, but not continuously; rather, the patterns appear intermittently in patches. With a further increase in the external force, the system exhibits unpredictable dynamics, indicating the presence of chaos in the dynamical system. Fig. (10–12) present two-dimensional, three-dimensional, and temporal profiles that correspond to periodic, quasi-periodic, and chaotic dynamics. Furthermore, we find the stability and multi stability using LE and MA, that are shown in Fig. (13-14), where the system has more than one stable states. Our solutions establish an understanding for dimension-building to examine pulse interactions, memory effects, and signal modulation in monomode optical fibers.

References

[1] Triki, H., Mirzazadeh, M., Ahmed, H. M., Samir, I., and Hashemi, M. S. (2023). Higher-order Sasa–Satsuma equation: Nucci's reduction and soliton solutions. The European Physical Journal Plus, 138(5), 1-10.

[2] Xue, S., and Zhang, G. (2023). Quasi-soliton control in optical lattices with longitudinal exponentially modulation. Optik, 287, 171106.

[3] Chen, H. X. (2022). Hadronic molecules in B decays. Physical Review D, 105(9), 094003.

[4] Ahmad, I., Jalil, A., Ullah, A., Ahmad, S., & De la Sen, M. (2023). Some new exact solutions of (4+ 1)-dimensional Davey–Stewartson-Kadomtsev–Petviashvili equation. Results in Physics, 45, 106240.

[5] Umer, M., and Olejnik, P. (2024). Symmetry-Optimized Dynamical Analysis of Optical Soliton Patterns in the Flexibly Supported Euler–Bernoulli Beam Equation: A Semi-Analytical Solution Approach. Symmetry, 16(7), 849.

[6] Seadawy, A. R., & Ali, A. (2023). Novel wave behaviors of the generalized Kadomtsev–Petviashvili modified equal width-burgers equation via modified mathematical methods. International Journal of Modern Physics B, 37(20), 2350198.

[7] H. M. Baskonus and H. Bulut, Exponential prototype structures for (2+1)-dimensional Boiti-Leon-Pempinelli systems in mathematical physics, Wave Random Complex Media 26 (2016), no. 2, 189–196.

[8] W. X. Ma and Y. Zhou, Lump solutions to nonlinear partial differential equations via Hirota bilinear forms, J. Differ. Eq. 264 (2018), 2633– 2659.

[9] I. Ahmad, M. N. Khan, M. Inc, H. Ahmad, and K. S. Nisar, Numerical simulation of simulate an anomalous solute transport model via local meshless method, Alex. Eng. J. 59 (2020), 2827–2838.

[10] S. Kumar, W. X. Ma, S. K. Dhiman, and A. Chauhan, Lie group analysis with the optimal system, generalized invariant solutions, and an enormous variety of different wave profiles for the higher-dimensional modified dispersive water wave system of equations, Eur. Phys. J. Plus 138 (2023), no. 5, 434.

[11] A. M. Wazwaz, New travelling wave solutions of different physical structures to generalized BBM equation, Phys. Lett. A. 355 (2006), 358–362.

[12] Khater, M. M., Seadawy, A. R., & Lu, D. (2018). Optical soliton and rogue wave solutions of the ultra-short femto-second pulses in an optical fiber via two different methods and its applications. Optik, 158, 434-450.

[13] Singh, S., Kaur, L., Sakthivel, R., & Murugesan, K. (2020). Computing solitary wave solutions of coupled nonlinear Hirota and Helmholtz equations. Physica A: Statistical Mechanics and its Applications, 560, 125114.

[14] K. L. Wang, New solitary wave solutions and dynamical behaviors of the nonlinear fractional Zakharov system, Qualitative Theory Dynam. Syst. 23 (2024), 98.

[15] K. J. Wang, Resonant multiple wave, periodic wave and interaction solutions of the new extended (3+1)-dimensional Boiti-Leon-MannaPempinelli equation, Nonlinear Dynam. 111 (2023), 16427–16439, DOI 10.1007/s11071-023-08699-x.

[16] B. Ghanbari and D. Baleanu, Applications of two novel techniques in finding optical soliton solutions of modified nonlinear schrÖdinger equations, Results Phys. 44 (2023), 106171.

[17] M. Srivastava, H., Günerhan, H., Ghanbari, B. (2019). Exact traveling wave solutions for resonance nonlinear Schrödinger equation with intermodal dispersions and the Kerr law nonlinearity. Mathematical Methods in the Applied Sciences, 42(18), 7210-7221.

[18] Hossain, A. K. S., and Akbar, M. A. (2021). Traveling wave solutions of Benny Luke equation via the enhanced (G'/G)-expansion method. Ain Shams Engineering Journal, 12(4), 4181-4187.

[19] Saifullah, S., Ahmad, S., Alyami, M. A., and Inc, M. (2022). Analysis of interaction of lump solutions with kink-soliton solutions of the generalized perturbed KdV equation using Hirota-bilinear approach. Physics Letters A, 454, 128503.

[20] Novikov, S., Manakov, S. V., Pitaevskii, L. P., and Zakharov, V. E. (1984). Theory of solitons: the inverse scattering method. Springer Science and Business Media.

[21] Roshid, H. O. (2017). Novel solitary wave solution in shallow water and ion acoustic plasma waves in-terms of two nonlinear models via MSE method. Journal of Ocean Engineering and Science, 2(3), 196-202.

[22] Kumar, S., and Rani, S. (2022). Study of exact analytical solutions and various wave profiles of a new extended (2+ 1)-dimensional Boussinesq equation using symmetry analysis. Journal of Ocean Engineering and Science, 7(5), 475-484.

[23] Jimbo, M., and Miwa, T. (1983). Solitons and infinite dimensional Lie algebras. Publications of the Research Institute for Mathematical Sciences, 19(3), 943-1001.

[24] Ohta, Y., Wang, D. S., and Yang, J. (2011). General N-dark–dark solitons in the coupled nonlinear Schrödinger equations. Studies in Applied Mathematics, 127(4), 345-371.

[25] Ohta, Y., and Yang, J. (2012). General high-order rogue waves and their dynamics in the nonlinear Schrödinger equation. Proceedings of the Royal Society A: Mathematical, Physical and Engineering Sciences, 468(2142), 1716-1740.

[26] Feng, B. F. (2014). General N-soliton solution to a vector nonlinear Schrödinger equation. Journal of Physics A: Mathematical and Theoretical, 47(35), 355203.

[27] Dey, P., Sadek, L. H., Tharwat, M. M., Sarker, S., Karim, R., Akbar, M. A., and Osman, M. S. (2024). Soliton solutions to generalized (3+ 1)-dimensional shallow water-like equation using the $(\phi'/\phi, 1/\phi)$-expansion method. Arab Journal of Basic and Applied Sciences, 31(1), 121-131.

[28] Rasid, M. M., Miah, M. M., Ganie, A. H., Alshehri, H. M., Osman, M. S., and Ma, W. X. (2024). Further advanced investigation of the complex Hirota-dynamical model to extract soliton solutions. Modern Physics Letters B, 38(10), 2450074.

[29] Chou, D., Boulaaras, S. M., Rehman, H. U., Iqbal, I., Akram, A., and Ullah, N. (2024). Additional investigation of the Biswas–Arshed equation to reveal optical soliton dynamics in birefringent fiber. Optical and Quantum Electronics, 56(4), 705.

[30] Kumar, S., and Kumar, A. (2023). Newly generated optical wave solutions and dynamical behaviors of the highly nonlinear coupled Davey-Stewartson Fokas system in monomode optical fibers. Optical and Quantum Electronics, 55(6), 566.

[31] Khater, M. M. (2021). Analytical simulations of the Fokas system; extension (2+ 1)-dimensional nonlinear Schrödinger equation. International Journal of Modern Physics B, 35(28), 2150286.

[32] Chen, T. T., Hu, P. Y., and He, J. S. (2019). General higher-order breather and hybrid solutions of the Fokas system. Communications in Theoretical Physics, 71(5), 496.

[33] Ohta, Y., and Yang, J. (2013). Dynamics of rogue waves in the Davey–Stewartson II equation. Journal of Physics A: Mathematical and Theoretical, 46(10), 105202.

[34] Fokas, A. S., and Santini, P. M. (1990). Dromions and a boundary value problem for the Davey-Stewartson 1 equation. Physica D: Nonlinear Phenomena, 44(1-2), 99-130.

[35] Selima, E. S., Seadawy, A. R., and Yao, X. (2016). The nonlinear dispersive Davey-Stewartson system for surface waves propagation in shallow water and its stability. The European Physical Journal Plus, 131, 1-16.

[36] Rehman, H. U., Said, G. S., Amer, A., Ashraf, H., Tharwat, M. M., Abdel-Aty, M., ... and Osman, M. S. (2024). Unraveling the (4+ 1)-dimensional Davey-Stewartson-Kadomtsev-Petviashvili equation: Exploring soliton solutions via multiple techniques. Alexandria Engineering Journal, 90, 17-23.

[37] Ma, M., Mihalache, D., Zhou, F., Chen, S. A., He, J., and Rao, J. (2024). Bright solitons on periodic background in the nonlocal Davey–Stewartson I equation with fully space-shifted PT-symmetry. Nonlinear Dynamics, 1-20.

[38] Kumar, S., & Kumar, A. (2023). Newly generated optical wave solutions and dynamical behaviors of the highly nonlinear coupled Davey-Stewartson Fokas system in monomode optical fibers. Optical and Quantum Electronics, 55(6), 566.